CAMBRIDGE
UNIVERSITY PRESS

Article

Grain-scale distribution of molybdenite polytypes versus rhenium contents: µXRD and EBSD data

Olga Y. Plotinskaya[1]* , Vladimir V. Shilovskikh[2] , Jens Najorka[3], Elena V. Kovalchuk[1], Reimar Seltmann[3] and John Spratt[3]

[1]Institute of Geology of Ore Deposits, Petrography, Mineralogy, and Geochemistry Russian Academy of Sciences (IGEM RAS), Staromonetny per. 35, Moscow 119017, Russia; [2]Saint Petersburg State University, Ulyanovskaya ul. 1, Saint-Petersburg 198504, Russia; and [3]Natural History Museum, London SW7 5BD, UK

Abstract

Molybdenite from two porphyry copper mineralisation sites within the South Urals was studied by electron microprobe (EMPA), micro x-ray diffraction (µXRD) and electron backscattered diffraction (EBSD) methods. Elevated contents of rhenium (0.2 to 0.4, sometimes up to 1.1 wt.%) form linear zones from several to tens of micrometres wide and up to hundreds of micrometres long parallel to the elongation of molybdenite flakes. In most cases Re-rich zones are composed of the rhombohedral (3*R*) polytype of molybdenite, while the rest of the molybdenite flakes with ca. 0.1 wt.% of Re consist of hexagonal (2*H*) molybdenite. In rare cases Re-rich zones are confined to grain boundaries of molybdenite-2*H*. It is shown that both µXRD and EBSD are the most appropriate tools to distinguish different polytypes within a single grain of molybdenite.

Introduction

Molybdenite is the primary carrier of rhenium, which is an important critical metal in the United Kingdom and Russian Federation (Chakhmouradian *et al.*, 2015 and references therein). This makes the study of both structural and chemical heterogeneity of molybdenite extremely important. Heterogeneous distribution of rhenium, and, sometimes, tungsten and selenium in molybdenite have been identified by electron microprobe analysis (EMPA) (Kovalenker *et al.*, 1974; Prokof'ev *et al.*, 2007; Voudouris *et al.*, 2009, 2019; Grabezhev and Shagalov, 2010; Grabezhev, 2013; Grabezhev and Voudouris, 2013; Kalinin *et al.*, 2013; Maksimyuk and Kulikova, 2013; Grabezhev and Hiller, 2015; Plotinskaya *et al.*, 2015, 2018*a*; Rathkopf *et al.*, 2017; McFall *et al.*, 2019), by laser ablation inductively coupled plasma mass spectrometry (LA-ICPMS) (Aleinikoff *et al.*, 2012; Ciobanu *et al.*, 2013; Bogdanov and Krumov, 2016; Kovalenker *et al.*, 2018, Plotinskaya *et al.*, 2018*a*), and by nanoscale secondary ion mass spectrometry (NanoSIMS) (Barra *et al.*, 2017).

Newberry (1979) revealed the positive correlation between contents of rhenium and the portion of rhombohedral (3*R*) polytype in molybdenite. Later Filimonova *et al.* (1984) made similar observations. The 3*R* polytype has since been considered more favourable for Re incorporation than the more common hexagonal (2*H*) polytype, although sometimes high Re contents (>1wt.%) have been reported both in natural (Voudouris *et al.*, 2009) and synthetic (Drabek *et al.*, 2010) 2*H* molybdenites. It is notable that all papers

mentioned above analysed bulk samples to estimate the 3*R*/2*H* ratio in molybdenite and did not take into account the chemical and structural heterogeneity of individual molybdenite grains.

The present paper is the first attempt to identify the distribution of different polytypes of molybdenite within a single grain using only non-destructive methods, such as micro x-ray diffraction (µXRD) and electron back-scattered diffraction (EBSD), and to reveal the relationships between variations of rhenium contents and molybdenite structure.

Sample selection and analytical methods

Sample selection

Molybdenite grains selected for this study were chosen according to the following conditions: (1) should form flakes large enough to be analysed, i.e. at least tens of µm; (2) must be neither mechanically deformed nor subjected to post-depositional hydrothermal or supergene alteration; (3) should have Re contents (i) easily detectable by EMPA (i.e. > 0.1 wt.%) and (ii) highly variable; and (4) must consist of both 3*R* and 2*H* polytypes.

For the above mentioned reasons two molybdenite-bearing samples from porphyry copper mineralisation of the Southern Urals were selected.

Sample Z-1461/164.5 comes from the Zapadnoe deposit located immediately to the west from the Mikheevskoe porphyry copper deposit, Chelyabinsk Oblast, Russia. The latter was described by Plotinskaya and co-workers (Plotinskaya *et al.*, 2015, 2018*b*). The sample represents seriate diorite porphyry with phyllic alteration and a network of quartz veinlets ~0.5 cm thick with molybdenite nests up to 2 mm and later chlorite stringers. Molybdenite forms in bunches of sub-parallel flakes tens to
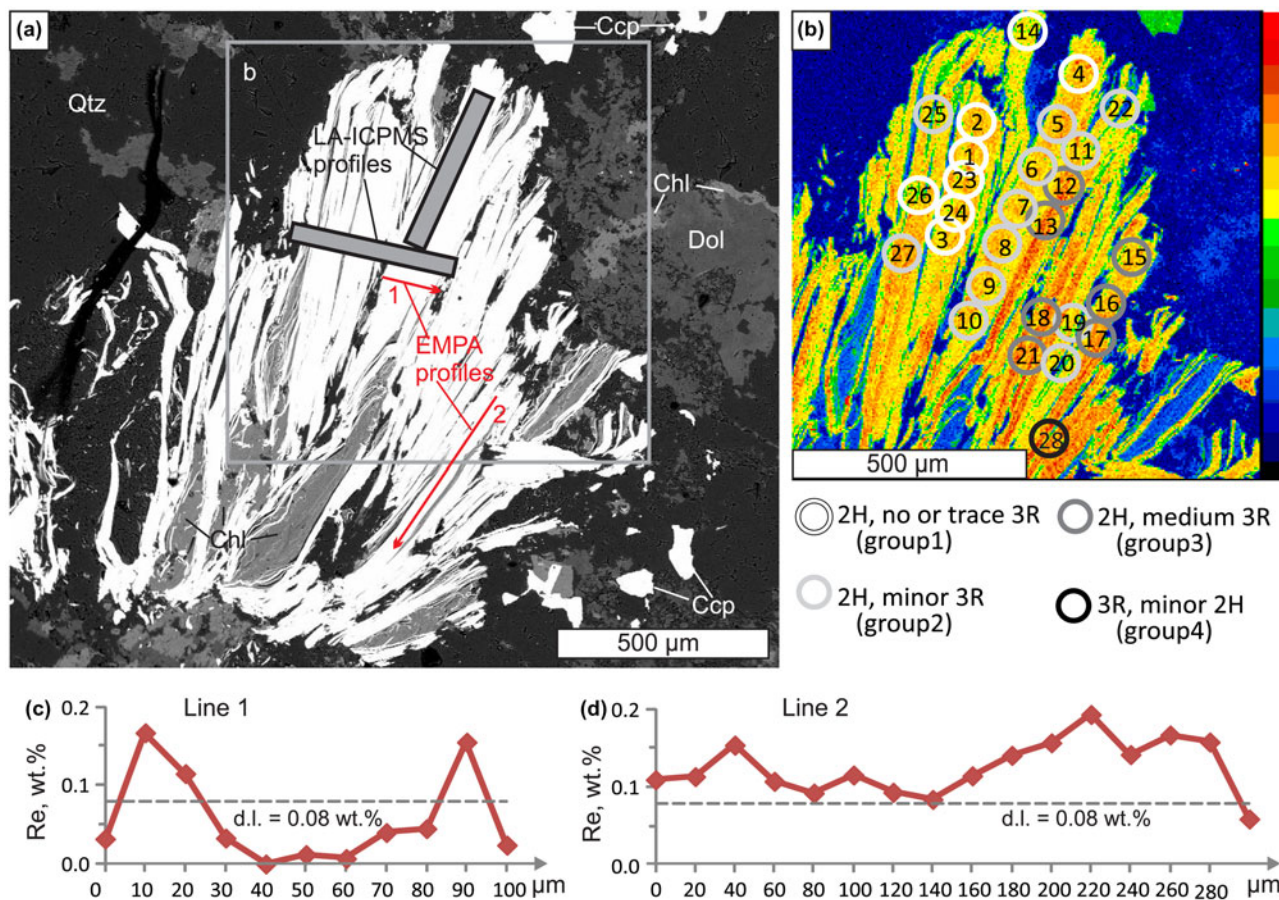
Fig. 1. Molybdenite from sample Z-1461/164.5 showing the position of EMPA profiles and μXRD spot analyses (note that the effective area of μXRD analysis is larger and shown schematically). (*a*) Back-scattered electron image; (*b*) Re*L*α X-ray map, (*c*) and (*d*) variation of Re contents along EMPA profiles.

100 μm wide and 500 to 700 μm long. Flakes are intergrown with chlorite and overgrown by quartz with minor dolomite (Fig. 1).

Sample Bir-1101/291.2 comes from the Birgilda porphyry copper sub-economic deposit, also in Chelyabinsk Oblast (54°59′47″N, 61° 5′17″E). Its geology as well as molybdenite assemblages and trace-element geochemistry (studied by EMPA and LA-ICPMS) were described by Plotinskaya *et al.* (2018*a*). The sample is aphyric basalt with pervasive chlorite alteration, numerous epidote–pyrite stringers and veinlets of white quartz with large pyrite nests and small nests of molybdenite. Molybdenite is present as aggregates of irregularly oriented flakes (Figs 2 to 4). Individual flakes are from 10 to 80 μm across and 50 to 150 μm long, intergrown with quartz, pyrite, epidote, albite, K-feldspar and chalcopyrite (Plotinskaya *et al.*, 2018*a*).

Electron microprobe analysis

The EMPA study was performed with a JEOL JXA-8200 electron microprobe equipped with five wavelength-dispersive (WDX) spectrometers at the 'IGEM-Analitika' shared analytical centre, Moscow, Russia (analysts: E.V. Kovalchuk and V.I. Taskaev). The operating conditions were: beam diameter 1 μm, accelerating voltage 20 kV and beam current 20 nA. Counting times were: 10 s for Mo, S and Se; 30 s for W; and 50 s for Re. Analytical lines were Re*M*β, Mo*L*α, W*L*α, Se*L*α, and S*K*α. The following standards were used: MoS_2 (Mo and S), metallic rhenium (Re), scheelite (W) and CdSe (Se). The *ZAF* procedure within the *JEOL* software was used for matrix correction. The detection limits (3σ) were

0.08 wt.% for Re and Se, and 0.09 wt.% for W. Calibrated maps of Re contents were obtained with the following conditions: 20 kV (acceleration voltage), 20 nA (beam current) and 200 ms (dwell time) per spot. Non-calibrated X-ray maps of the sample Z-1461/164.5 were obtained using a Cameca SX-100 electron microprobe with five WDX spectrometers (Natural History Museum, London, UK) using Re*L*α, Re*M*α, Mo*L*α, S*K*α, Ca*K*α, Si*K*α, Fe*K*α and Zn*K*α analytical lines.

Micro X-ray diffraction study

The micro X-ray diffraction study was performed using a Rigaku Rapid II micro-diffraction system, equipped with a Cu X-ray source, a carbon monochromator, a 2D curved image plate detector and an adjustable *XY* stage (Natural History Museum, London, UK). X-ray diffraction patterns were collected using a 30 μm X-ray beam collimator. The effective area of the μXRD analysis depended on the sample orientation to the beam. Stage oscillation about the ω axis (20–27°2θ) and spinning about the φ axis produced a maximum beam footprint of 90 μm on the sample. The polytype proportion was estimated using the integrated intensity ratio of peaks at 39.5 and 41.1°2θ, respectively 103 and 015 for 2*H* and 3*R*. These peaks were selected because they are intense, well separated, and fitting of the areal intensities is not much affected by peak overlap. As peak intensities can vary because of non-ideal diffraction conditions the obtained 3*R*/2*H* ratios should be considered semi-quantitative.
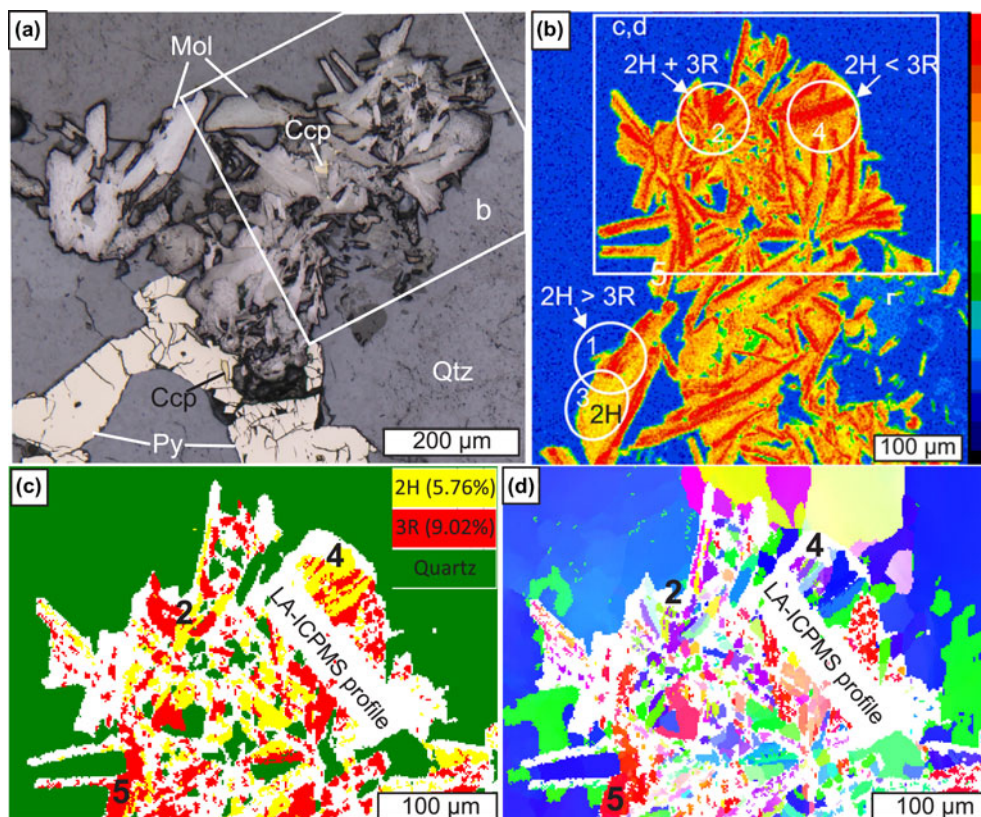
Fig. 2. Molybdenite from sample Bir-1101/291.2, site 1. (a) and (b) modified after (Plotinskaya *et al.*, 2018*a*). (a) Molybdenite (Mol) intergrown with pyrite (Py) and chalcopyrite (Ccp) in quartz (Qtz), reflected light; (b) enlarged part of (a), ReLα X-ray map, circles show μXRD analyses; (c) and (d) EBSD data (1.5 μm step): (c) phase map showing the distribution of 2H and 3R polytypes; (d) inverse-pole figure map showing different orientations in colours relative to the X_0 direction.

Electron back-scatter diffraction study

All samples were treated previously with Ar plasma via Oxford IonFab300 plasma etcher (10 min exposure, 500 V accelerating voltage and 200 mA beam current) at the SPbU, 'Nanophotonics' centre (Saint-Petersburg, Russia). The electron back-scatter diffraction study was carried out with a Hitachi S-3400N electron microscope equipped with Oxford NordlysNano EBSD detector at the SPbU, 'Geomodel' centre (Saint-Petersburg, Russia). Operating conditions were: 30 kV (accelerating voltage), 1 nA (beam current) and 0.5 s (dwell time), giving a diffraction pattern (Kikuchi image) of 1344×1024 pixels. All the acquired Kikuchi images were processed automatically with *AZtecHKL* software (Oxford Instruments) and compared to theoretical images generated from molybdenite-2H and -3R structural data (Persson, 2014, 2016). Best fit to the experimental data was chosen in a competitive mode. Noise reduction was performed, phase and orientation maps as well as pole figures were created using Oxford *Channel5* software.

Results

Electron microprobe analysis

In all sites of the two samples studied, X-ray mapping revealed Re-enriched zones from several μm to tens of μm wide and up to hundreds of μm long. Such zones are confined to either axial or marginal parts of molybdenite flakes and are always parallel to the elongation of molybdenite flakes (Figs 1*b*, 2*b*, 3*b* and 4*b*). Analysed points (Figs. 1*c,d*, 3*c*, 4*d,j*, Appendix 1, see supplementary

data below) show Re contents from 0.15 to 0.4 wt.% (sometimes up to 0.6 wt.%) within such zones and from below detection limit (b.d.l.) to 0.1 wt.% of Re outside of them. Our previous studies of the site 1 sample Bir-1101/291.2 (Plotinskaya *et al.*, 2018*a*) revealed similar results with up to 1.1 wt.% of Re. Tungsten and Se contents are below the detection limit in both samples studied.

Micro X-ray diffraction data

Twenty eight analyses were obtained for sample Z-1461/164.5. The analysis locations are shown on the Fig. 1*b*. Based on 3R to 2H polytype proportion the XRD patterns were sorted into four groups: group 1 where only traces or no 3R polytype were detected (8 spots), group 2 with a 3R/2H ratio 0.07 to 0.25 (12 spots), group 3 with a 3R/2H ratio 0.3 to 1.2 (7 spots), and one spot with 3R/2H = 3.6 (Appendix 2).

For sample Bir-1101/291.2 four XRD patterns were collected only from site 1. Both 2H and 3R polytypes are present in areas 1, 2 and 4 (Fig. 2*b*). In the latter area the 3R polytype is predominant, while area 3 contains mostly the 2H polytype (Appendix 2).

Electron back-scattered diffraction data

Phase maps (Figs 2*c*, 3*d*, 4*c* and *h*) show that in all four sites of sample Bir-1101/291.2 molybdenite is represented by both 2H and 3R polytypes. In site 1, the 3R polytype dominates over 2H (9% and 5.8% respectively) while in sites 2, 3 and 4 the 3R polytype is less abundant than 2H (2.6 and 4.2% within site 2, 10.4 and 18.4% within site 3 and 1.4 and 21.2% within site 4
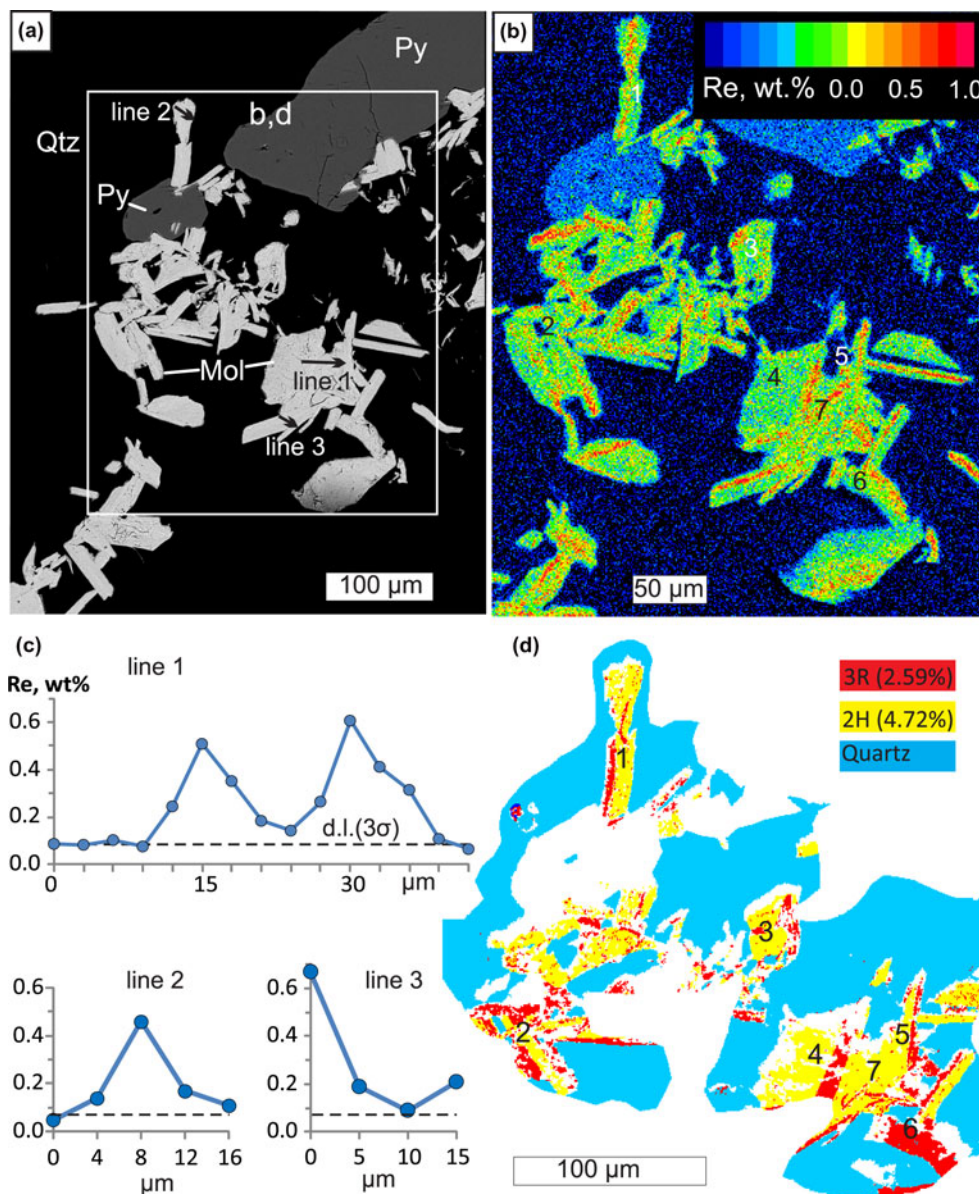
Fig. 3. Molybdenite from sample Bir-1101/291.2, site 2. (*a*) Molybdenite intergrown with pyrite in quartz, backscattered electron image; (*b*) calibrated map of Re content (wt.%); (*c*) EMPA profiles; (*d*) EBSD phase map (0.5 μm step) showing the distribution of 2*H* and 3*R* polytypes.

respectively). The inverse pole figure (IPF) maps of crystal orientations show no predominant colour in all four sites (Figs 2*d*, 4*e*, *i*), implying that molybdenite flakes do not have a crystallographic preferred orientation.

## Discussion

Note on data quality

It has been noted earlier (Shilovskikh *et al.*, 2019) that previous sample treatment, especially LA-ICPMS analysis and, to a lesser degree, X-ray mapping, reduces the quality of EBSD maps. Indeed, the EBSD map of site 1 sample Bir-1101/291.2 was obtained after X-ray mapping and LA-ICPMS analysis (Plotinskaya *et al.*, 2018*a*) and this resulted in a lower quality of both phase map (Fig. 2*c*) and IPF map (Fig. 2*d*) due to the high portion of non-indexed areas (white colour on Fig. 2*c,d*). In sites

2, 3 and 4, where EBSD data were collected before X-ray mapping, the EBSD maps show an improved quality (Figs 3*d*, 4*c,e,h,i*).

On the contrary, μXRD data collected after X-ray mapping and LA-ICPMS analysis in both samples studied are not affected by any previous treatment. Moreover, good quality XRD patterns were obtained directly from laser traces (e.g. spots 4 to 7 on Fig. 1*b*). The individual intensities of most peaks in the patterns match well with the reference lines. This indicates that the data obtained can be treated identically to conventional powder data and that peak intensities as well as peak ratios are suitable for comparison.

Correlation between Re content in molybdenite and abundance of the 3R polytype

In sample Bir-1101/291.2 the highest Re content (0.3 to 1.1 wt.%) was reported within site 1 where EBSD data showed the
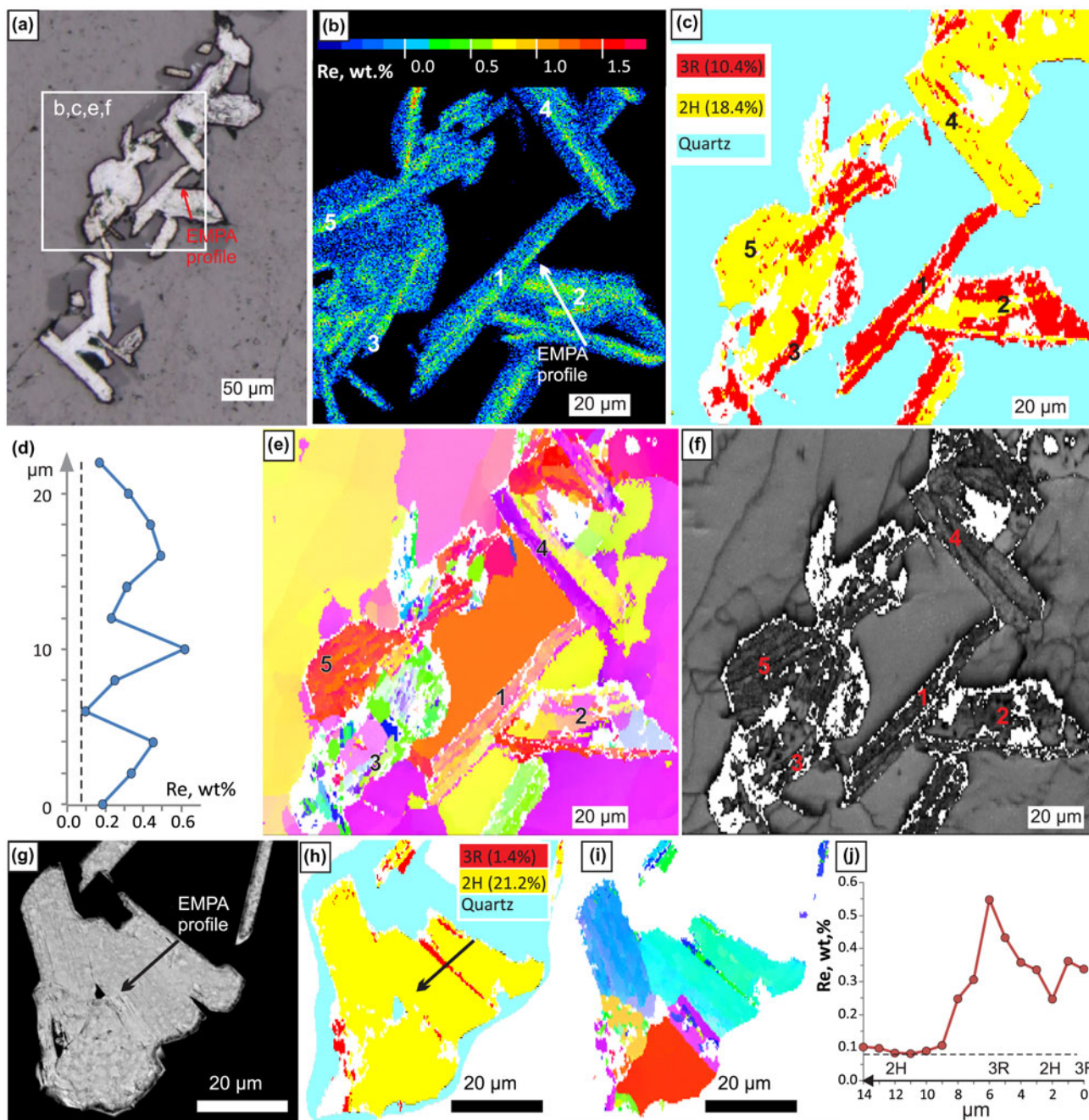
Fig. 4. Molybdenite from sample Bir-1101/291.2, site 3 (*a–f*) and site 4 (*g–j*). (*a*) Molybdenite in quartz, reflected light; (*b*) enlarged part of (*a*), calibrated map of Re content (wt.%); (*c*) EBSD phase map (0.5 μm step) showing the distribution of 2*H* and 3*R* molybdenite; (*d*) EMPA profile; (*e*) inverse pole figure map showing different orientations in colours relative to the Y_0 direction; (*f*) band contrast map; (*g*) back-scattered electron image; (*h*) EBSD phase map (0.25 μm step) showing the distribution of 2*H* and 3*R* polytypes; (*i*) IPF map showing different orientations in colours relative to the Z_0 direction; and (*j*) EMPA profile.

dominance of the 3*R* polytype (Fig. 2*c*). In sites 2 and 3, where 2*H* is almost twice as abundant Re contents are mostly from b.d.l. to 0.4 wt.% and occasionally up to 0.6 wt.% (Figs 3 and 4*b–d*). μXRD revealed the same within site 1, where area 3 is featured by the lowest Re content and an absence of 3*R* polytype (Fig 2*b* and *c*). This means the abundance of 3*R* polytype and Re content correlate in different sites within a sample scale.

Within a grain scale, as observed in sample Z-1461/164.5 (Fig. 1*b*), zones with elevated Re contents are composed either of 3*R* polytype (e.g. spot 28) or of both 3*R* and 2*H* polytypes in variable ratios.

In sample Bir-1101/291.2 a comparison of Re X-ray maps and EBSD phase maps show in most cases that Re-enriched zones are composed of the 3*R* polytype. Perfect coincidence between 3*R* polytype and zones with elevated Re contents can be observed in the site 1, areas 4, 2, and 5 (Fig. 2*b* and *c*), site 2, areas 1 to 6 (Fig. 3*b* and *d*), site 3, areas 1 to 3 (Fig. 4*b* and *c*) and in site 4 (Fig. 4 *h–j*).

Sometimes however no 3*R* polytype was detected in Re-rich molybdenite. These are: site 2, area 7 (Fig. 3*b* and *d*) and site 3, areas 4 and 5 (Fig. 4 *b,c,e,f*). One may suppose that in some cases the 3*R* polytype bands were thinner than the EBSD step size (0.25 to 1.5 μm) and were missed during mapping.

For example, a transmission electron microscopy study by Kovalenker *et al.* (2018) identified nanometre-sized interlayers of 3*R* polytype in 2*H* molybdenite. Some 'noise' in areas 4 and 5 of site 3 (Fig. 4*c*) indirectly supports this suggestion. In site 3, area 4 however a Re-rich 'band' is confined to a grain boundary which can be seen both on the orientation map and the band contrast map (Fig. 4 *e,f*). In area 5 (site 3) very small grains misorientated relative to the Y_0 direction can be observed (Fig. 4*e*). On the band contrast map (Fig. 4*f*) however area 4 represents a patch of parallel molybdenite grains. This suggests elevated Re contents in 2*H* molybdenite are confined to grain boundaries.

Summary

A combination of EMPA, µ-XRD and EBSD methods show that in most cases zones with an elevated Re content are composed of 3*R*-polytype molybdenite; in rare cases such zones are confined to boundaries of 2*H*-polytype molybdenite flakes.

The most appropriate tool to distinguish different polytypes within a single grain of molybdenite is EBSD. It is however sensitive to previous treatment such as X-ray mapping and LA-ICPMS. µXRD is less informative because of the large beam size but, it is useful for the preliminary evaluation and selection of grains for further investigation. Moreover, the data quality of µXRD is much less affected by any previous treatment and it can be applied after X-ray mapping and LA-ICPMS analysis.

References

Aleinikoff J.N., Creaser R.A., Lowers H.A., Magee C.W. and Grauch R.I. (2012) Multiple age components in individual molybdenite grains. *Chemical Geology*, **300–301**, 55–60.

Barra F., Deditius A., Reich M., Kilburn M.R., Guagliardo P., and Roberts M.P. (2017) Dissecting the Re–Os molybdenite geochronometer. *Scientific Reports*, **7**, 16054.

Bogdanov K. and Krumov I. (2016) Trace element vectors in molybdenite from porphyry-copper deposits of Bulgaria. *Bulgarian Geological Society, National Conference with International Participation GEOSCIENCES 2016*, pp. 17–18.

Chakhmouradian A.R., Smith M.P., and Kynicky J. (2015) From "strategic" tungsten to "green" neodymium: A century of critical metals at a glance, *Ore Geology Reviews*, **64**, 455–458.

Ciobanu C.L., Cook N.J., Kelson C.R., Guerin R., Kalleske N. and Danyushevsky L. (2013) Trace element heterogeneity in molybdenite fingerprints stages of mineralization. *Chemical Geology*, **347**, 175–189.

Drabek M., Rieder M. and Bohmova V. (2010) The Re–Mo–S system: new data on phase relations between 400 and 1200°C. *European Journal of Mineralogy*, **22**, 479–484.

Filimonova L.E., Zhukov N.M. and Malyavskaya A.T. (1984) The genetic aspects of polytypes and content of Re in molybdenite at the porphyry copper deposits. *Geokhimiya*, **7**, 1040–1046 [in Russian].

Grabezhev A.I. (2013) Rhenium in porphyry copper deposits of the Urals. *Geology of Ore Deposits*, **55**, 13–26.

Grabezhev A.I. and Hiller V.V. (2015) Rhenium in molybdenite of Tominsk porphyry copper deposit (the South Urals): Results of the microprobe study. *Proceedings of the Russian Mineralogical Society*, **CXLIV**, 81–93 [in Russian with an English abstract].

Grabezhev A.I. and Shagalov E.S. (2010) Rhenium distribution in molybdenite: results of microprobe scanning (porphyry copper deposits, the Urals). *Doklady Earth Sciences*, **431**, 351–355.

Grabezhev A.I. and Voudouris P.C. (2015) Rhenium distribution in molybdenite from the Vosnesensk porphyry Cu ± (Mo,Au) deposit (Southern Urals, Russia). *The Canadian Mineralogist*, **52**, 671–686.

Kalinin A.A., Savchenko Ye.E. and Selivanova E.A. (2013) Rhenium- and selenium-bearing molybdenite in Ozernoye ore occurrence in Salla-Kuolajarvinskaya zone. *Northern Karelia.* Proceedings of the Russian Mineralogical Society, **142**, 104–114 [in Russian with English abstract].

Kovalenker V.A., Laputina I.P. and Vyalsov L.N. (1974) On rhenium-rich molybdenite from the Talnakh copper–nickel deposit, Norilsk district. *Doklady AN SSSR*, **217**, 187–189 [In Russian].

Kovalenker V.A., Trubkin N.V., Abramova V.D., Plotinskaya O.Yu., Kiseleva G.D., Borisovskii S.E., and Yazykova Yu.I. (2018) Typomorphic characteristics of molybdenite from the Bystrinskoe Cu–Au skarn-porphyry deposit, Eastern Transbaikalia, Russia. *Geology of Ore Deposits*, **60**, 62–81.

Maksimyuk I.E. and Kulikova I.M. (2013) Species of rhenium in molybdenite from various type ore deposits, *Proceedings of the Russian Mineralogical Society*, **142**, 94–106 [in Russian with an English abstract].

McFall K., Roberts S, McDonald I., Boyce A.J.Naden J., and Teagle D. (2019) Rhenium enrichment in the Muratdere Cu-Mo (Au-Re) rorphyry deposit, Turkey: evidence from stable isotope analyses (δ34S, δ18O, δD) and laser ablation-inductively coupled plasma-mass spectrometry analysis of sulfides, *Economic Geology.* https://doi.org/10.5382/econgeo.4638

Newberry R.J.J. (1979) Polytypism in molybdenite (I): a nonequilibriun impurity induced phenomenon. *American Mineralogist*, **64**, 758–767.

Persson K. (2014) Materials Data on MoS$_2$ (SG:160) by Materials Project. United States Department of Energy. https://doi.org/10.17188/1190621.

Persson K. (2016) Materials Data on MoS$_2$ (SG:194) by Materials Project. United States Department of Energy. https://doi.org/10.17188/1202268.

Plotinskaya O.Yu., Grabezhev A.I., and Seltmann R. (2015) Rhenium in ores of the Mikheevskoe Mo-Cu porphyry deposit, South Urals. *Geology of Ore Deposits*, **57**, 118–132.

Plotinskaya O.Y., Abramova V.D., Groznova E.O., Tessalina S.G., Seltmann R., Spratt J. (2018a) Trace element geochemistry of molybdenite from porphyry Cu deposits of the Birgilda-Tomino ore cluster (South Urals, Russia). *Mineralogical Magazine*, **82(S1)**, S281–S306.

Plotinskaya O.Y., Azovskova O.B., Abramov S.S., Groznova E.O., Novoselov K.A., Seltmann R., Spratt J. (2018b) Precious metals assemblages at the Mikheevskoe porphyry copper deposit (South Urals, Russia) as proxies of epithermal overprinting. *Ore Geology Reviews*, **94**, 239–260.

Prokof'ev V.Y., Zorina L.D., Kovalenker V.A., Akinfiev N.N., Baksheev I.A., Krasnov A.N., and Trubkin N.V. (2007). Composition, formation conditions, and genesis of the Talatui gold deposit, the Eastern Transbaikal region, Russia. *Geology of Ore Deposits*, **49**, 31–68.

Rathkopf C., Mazdab F., Barton I. and Barton M.D. (2017) Grain-scale and deposit-scale heterogeneity of Re distribution in molybdenite at the Bagdad porphyry Cu–Mo deposit, Arizona. *Journal of Geochemical Exploration*, **178**, 45–54.

Shilovskikh V.V., Plotinskaya O.Y., and Lozhkin M.S. (2019) Influence of the sample investigation story on the results of electron backscattered diffraction; molybdenite as example. Pp. 312–315 in: *Metallogeny of Ancient and Modern Oceans*. Institute of Mineralogy UB RAS, Miass, Russia.

Voudouris P.C., Melfos V., Spry P.G., Bindi L., Kartal T., Arikas K., Moritz R. and Ortelli M. (2009) Rhenium-rich molybdenite and rheniite in the Pagoni Rachi Mo-Cu-Te-Ag-Au prospect, Northern Greece: Implications for the Re Geochemistry of porphyry style Cu-Mo and Mo mineralization. *The Canadian Mineralogist*, **47**, 1013–1036.

Voudouris P.C., Mavrogonatos C., Melfos V., Spry P.G., Magganas A., Alfieris D., Soukis K., Tarantola A., Periferakis A., Kołodziejczyk J., Scheffer C., Repstock A. and Zeug M. (2019) The geology and mineralogy of the Stypsi porphyry Cu-Mo-Au-Re prospect, Lesvos Island, Aegean Sea, Greece. *Ore Geology Reviews*, https://doi.org/10.1016/j.oregeorev.2019.103023